https://doi.org/10.2352/ISSN.2169-4451.2020.36.108

Predicting Response of Printed Potentiometric Nitrate Sensors Using Image Based Machine Learning*

Qingyu Yang, Kerry Maize, Xin Jin, Hongjie Jiang, Muhammad Ashraful Alam, Rahim Rahimi, George T.C. Chiu, Ali Shakouri, Jan P. Allebach
Purdue University, West Lafayette, Indiana 47906, U.S.A.

Abstract

Solid-contact nitrate sensors have wide applications in agriculture. In manufacturing, fabrication is an essential step and strongly affects the sensor performance. We focus on controlling the fabrication process to develop an economical thin-film nitrate sensor with an ion-selective membrane (ISM). However, direct long-time measurement of sensor performance for monitoring fabrication is expensive and costs human labor. Thus, in this work, we propose an automatic system to predict the temporal potentiometric response based on non-contact images acquired in real time. Our prediction systems are generated by exploiting image-processing techniques and machine learning approaches. To improve the prediction accuracy, we also fuse manufacturing factors to the image inputs. The comparison of prediction performance with different inputs also helps us to understand their effects on the fabrication process.

Introduction

Nitrate sensors have been widely used to monitor soil conditions in real time. The Scalable Manufacturing of Aware and Responsive Thin Films (SMART) [1] consortium is developing an inexpensive mass-produced thin-film potentiometric nitrate sensor that can be manufactured with a roll-to-roll system. However, in the fabrication process of the nitrate sensor, a challenge is that the nonuniform coating of the ion-selective membrane (ISM) [2] is inevitable and affects the sensor performance a lot. Thus, we develop prediction systems to monitor the fabrication process efficiently.

Fig. 1 shows a 3D model of the SMART nitrate sensor. The electrode of the nitrate sensor is printed on a polyethylene terephthalate (PET) substrate with a coated ISM layer, and silicon passivation layer. The region of our interest is the area where the ISM contacts the electrode, which is called active region. It is worth mentioning that a conventional sensor performance analysis needs to put the sensor's active region in a nitrate solution and record the potentiometric response for around 24 hours. It is expensive and time-consuming to measure all the sensors individually to determine their performance metrics. To address this problem, a novel approach of exploiting machine learning techniques, which have powerful abilities of data analysis and model construction, is proposed to efficiently monitor and calibrate the fabrication process.

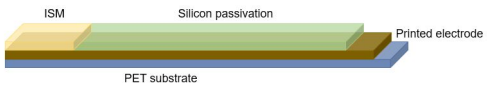

Figure 1. *3D model of the SMART nitrate sensor.*

*Research supported by the SMART Films consortium (https://engineering.purdue.edu/SMART-consortium).

In our previous work on image-based quality assurance for fabricated nitrate sensors [3], we realized the prediction of the end-time potential voltage of the measured potentiometric response based on a captured active-region image. The previous prediction verified the physical assumption that a relationship exists between the sensor images and sensor performance. However, the single value of the end-time voltage presents only limited information about the overall potentiometric response of the sensor. Also, we mentioned that the accuracy of the prediction has the potential to be improved.

In this paper, we continue to develop the prediction based on an active-region image. We exploit both traditional machine learning and deep learning to generate the image features and learn the non-linear relationships between the feature representations and the sensor performance curve. In our traditional machine learning approach, a local binary pattern (LBP) [4] descriptor is used to extract 1D texture features from the image. Then, we leverage support vector regression (SVR) [5] to find the non-linear relationship between the image features and the sensor performance metrics. Since convolutional neural networks (CNNs) have demonstrated their abilities to extract meaningful image representations and learn non-linear functions [6], we also implement a CNN to realize the prediction. In addition, we notice that there are some variations in manufacturing settings in the fabrication process within our dataset. According to the theoretical analysis, the thickness of the ISM from the sensor manufacturing process largely affects the ion-selective electrode's sensor performance [7]. In this paper, besides using the active-region images as inputs, we also fuse manufacturing factors to improve the prediction systems.

In particular, our contributions in this work are the following: (1) The previous dataset has been enlarged for the data-driven method implementation. (2) We propose the idea of interpolating the logarithmic function from the physics-model hypothesis to predict the large-scale 1D array of the sensor performance curve. (3) We exploit and compare two image-based methods, SVR with hand-crafted features and a deep network, to realize the prediction by addressing the non-linear regression task. (4) The varying manufacturing factors are fused with the image features to improve the accuracy of our prediction. In the reminder of this paper, we will describe our methods of dataset generation. Then, the designed systems for generating prediction models by traditional machine learning and deep learning will be presented and compared.

Dataset Generation

Our prediction system is designed to output the sensor performance curve based on an active-region image by a data-driven machine learning approach. The pre-processed 2D image of the nitrate sensor is the input to prediction system. Also, ground truth, which represents the sensor performance data, is required

to train the prediction model. Thus, we need to generate a consistent dataset, including the input active-region images and the ground truth.

Image Data Preparation

We use the same imaging system as in our previous work [3] to capture the sensor images. The imaging system consists of a fixed-focus digital microscope, a 0.5 × magnification telecentric lens, and a fiber optic illuminator. As Fig. 2 shows, the captured images are centered in the active regions with varying backgrounds. Since we only focus on the active region, we apply the Sobel operator [8], Otsu's algorithm [9], and subsequent morphological transformations to segment the active region. Then, the active-region images, which clearly show the varying roughness of the membranes, will be cropped to be our input images.

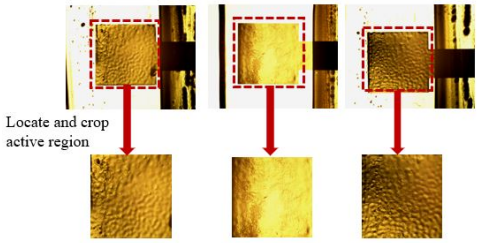

Figure 2. *Examples of image dataset preparation: the top part shows the captured images with the same resolution 1280 × 1024; the bottom part represents the cropped active-region images, which have size around 500 × 500 pixels.*

Ground Truth Data Generation

The system for generating ground truth data consists of two parts: potentiometric response measurement and data simplification. We obtain the sensor performance data by measuring the difference of potential voltages between our printed nitrate sensor and a reference sensor for around 24 hours [10]. Fig. 3 (a) shows the process of measuring one batch of sensors in nitrate solution. The physical model indicates that different concentrations of nitrate solution affect the sensor performance. Thus, we generate our dataset by measuring the potential voltages in 0.1 molar nitrate solutions as time increases from 0 to 24 hours to make it consistent. Fig. 3 (b) shows the sensor performance measurement for a batch of 16 sensors during this time window. Each measured performance curve is a large-scale 1D array, which consists of 1.5K to 2.5K points sampled at different time intervals.

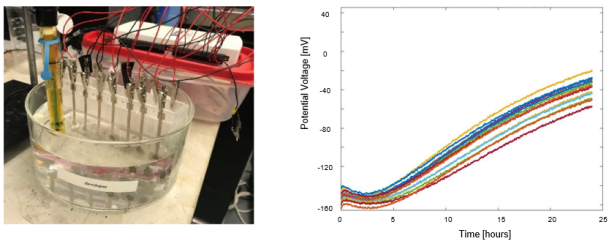

(a) (b)

Figure 3. *Measurement of the sensor performance of 16 sensors for around 24 hours: (a) measurement process; (b) recorded results.*

Since the measured sensor potentiometric response correlates to many sensor design parameters, a prediction that only depends on images is not reliable. Here, we introduce a physics-based model to simplify the temporal potentiometric response of the ion-selective sensor in the saturated phase. According to the generalized Nernst equation [7] that is derived from the first principle ion transport equation, the sensor output potential voltages follow a logarithmic relationship with time. Thus, we use a physics-based model to describe the behavior of the potential voltage V with increasing time t as shown in Eq. 1. Here, k is Boltzmann's constant, T represents temperature, and q is the concentration of the nitrates in the testing solution. Also, b represents the vertical shift of the curve, which is highly related to thickness and material variations of the fabricated membrane. In the ideal case, the values of k, T, and q are constant during a manufacturing run. But the sensor performance is also influenced by some non-ideal factors, such as moisture, an inner water layer, and secondary ion effects, etc. The non-ideal factors, however, are difficult to quantify based on the physical model. Thus, we simplify the raw data curve after saturation as a logarithmic curve V_{fit} with two parameters a and b, as shown in Eq. 2.

$$V(t) = \frac{kT}{q}\log(t) + b \tag{1}$$

$$V_{fit}(x_t) = a\log(x_t) + b \tag{2}$$

We preprocess the original measured data and use the above hypothesis to generate the best fitting logarithmic function with optimum parameters a and b. In particular, we smooth and downsample the large-scale vector of the original measured potential voltages V_m to a 100-element vector V_d. Only the last 80 points of V_d are considered as the potentiometric response in the saturated phase. Then, we apply a curve-fitting method to V_d to find a logarithmic curve with time-points ($x_t = 20, \ldots, 99$) that best fit it, called V_{fit}. Here, we use the Levenberg-Marquardt algorithm [11] to optimize the curve-fitting process. Fig. 4 shows two examples of the potentiometric response of the original measurement V_m, the smoothed data, the downsampled curve V_d, and the fitted curve V_{fit} in the saturated phase. In conclusion, the parameters a and b are the ground truth for our prediction to determine the sensor performance curve. We will introduce several methods to predict the parameters a and b based on the active-region images in the next section.

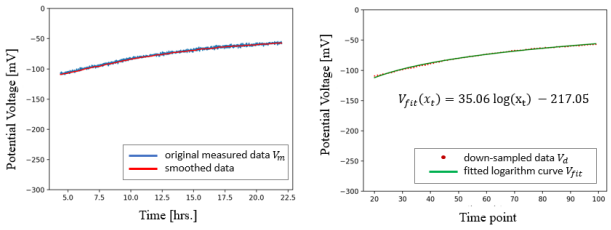

Figure 4. *Curve fitting example: the left-side figure shows the voltage response of the original measurement and the smoothed data as a function of time; the right-side figure shows the downsampled data points and the fitted curve V_{fit} vs. defined time points corresponding to the saturated phase. Here, a = 35.06, and b = -217.05.*

Methods of Prediction Based on Images

Based on the previously discussed physical model, the raw data of each sensor V_m is transformed to a logarithmic curve V_{fit}, which will be treated as the prediction target in our implementation. As shown in Eq. 2, two parameters a and b determine the shape of the V_{fit}. Therefore, the curve prediction task becomes a

two-output regression task. The overview of our system is shown in Fig. 5. Ground truth values for a and b are generated for each V_{fit}; and the training portion is used to supervise the learning process for the prediction system, which is a non-linear regression model. The inputs to the prediction system are images or feature vectors. The outputs are the predictions $\tilde{a}$ and $\tilde{b}$. In this section, we apply an SVR and a deep network as our non-linear regression models, and evaluate both performances.

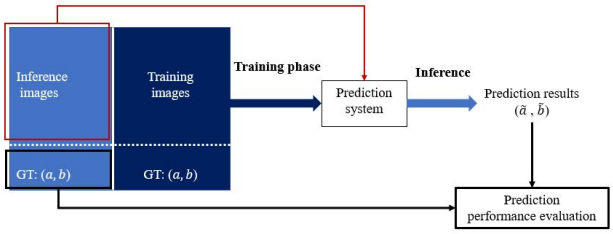

Figure 5. *Prediction system based on images via a machine learning approach.*

SVR with Hand-Crafted Features

SVR is an established machine learning method that can estimate the relationship between a high-dimensional feature space and a low-dimensional output space. To train the SVR, we firstly need to handcraft a 1D feature to describe the roughness of each active region. In the previous decade, the LBP descriptor has been commonly used to describe texture information, and achieved successful results in image classification [12]. Here, we use the circular LBP descriptor, as it is robust to rotation and illumination variations. Following [3], we extract a 9-element LBP array to represent the texture information.

After extracting image features, we exploit the SVR prediction model to find the approximate mapping from the handcrafted features to the output parameters. To be more specific, the extracted 1D LBP arrays in our training dataset are inputs to train the SVR. The conventional SVR establishes a linear/non-linear function from a high-dimensional input to a single value. In our case, the desired output is a pair of parameters a and b for each sensor. Thus, we train two independent SVRs for both a and b with shared inputs to construct a multi-output SVR system. As shown in Eq. 3, x_i represents the input feature vector, y_i is the single output, and w represents the coefficients of the regression model. In contrast to a least square regression, which minimizes the distance between target and prediction, SVR's objective function minimizes the L_2 norm of the coefficients w, subject to constraints. The constraints of the SVR have a hyper-parameter the margin ε. For the predictions that fall in the margin, the penalty is zero. The objective function also includes a term ζ_i, which penalizes the deviations of the predictions outside the margin. A hyper-parameter C is set to control the weight of the penalty for the deviation. By tuning the hyper-parameters C and ε, the SVR can obtain optimal performance. Since our previous experiments [3], using linear regression to predict the sensor performance, did not achieve a high accuracy, we consider that the relationship between the extracted features and the sensor performance is non-linear. Thus, we apply an radial basis function (RBF) kernel to the SVR [13] to handle the non-linearity.

$$\begin{aligned} &min\frac{1}{2}||w||^2 + C\sum_{i=1}^{n}|\zeta_i| \\ &constraints: |y_i - w^T x_i| \leq \varepsilon + |\zeta_i| \end{aligned} \tag{3}$$

Deep Learning Approach: Fine-tuning the CNN

In recent years, CNNs have demonstrated compelling performance for high-dimensional features extraction, image recognition, and image classification tasks [6]. In this work, we also leverage CNN to realize our prediction of the parameters a and b. In contrast to the SVR prediction tool based on the handcrafted features, we directly feed the 2D active-region images to the CNN. As shown in Fig. 6, the images with their corresponding ground truth data are used to tune the parameters of the CNN. We follow the physics-based model to compute the approximate potentiometric response with time points x_t. Here, x_t takes on the same values as before, which are 20, 21,..., 99. In each epoch, the L_2 loss between the predicted voltage vector $\tilde{V}_{fit}(x_t)$ and the ground-truth vector $V_{fit}(x_t)$ will backpropagate to tune the prediction model.

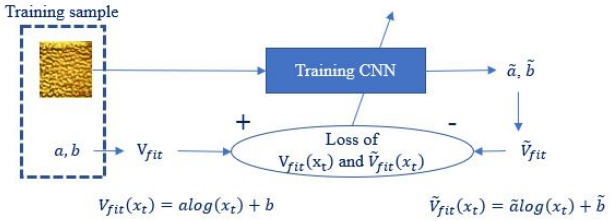

Figure 6. *System for training the CNN.*

We select ResNet-34 [14] as our backbone network. This network uses a residual learning strategy, which retains the learned features from the shallow layers to prevent the gradient from vanishing or exploding during the optimization. In general, the network has two main parts: convolutional layers and fully-connected (FC) layers. The convolutional layers are used to extract high dimensional features from the input images. Then, the FC layers regress the extracted features to the desired outputs. In addition, the ResNet also applies a global average pooling after the convolutional layers to reduce the dimension of the global representation. This pooling process can largely reduce the memory use and computations during the training process by taking the place of several FC layers in other networks, such as VGG [15] or AlexNet [16]. In the last layer, we change the output nodes of the original FC layer from 1000 to 2 for fitting the dimension of our desired outputs a and b. In addition, we replace the loss function cross-entropy loss, which is for image classification, by the L_2 loss, as we mentioned earlier for our regression task. In addition, we initialize our model with the weights pretrained on ImageNet [17] to yield faster convergence.

Fusion of Manufacturing Factors and Image Features

As we mentioned, the physics-based model indicates that the sensor performance also strongly depends on the thickness of the membrane. However, the active-region images that we used in the above methods do not contain thickness information. In addition, the thickness of the coating membrane is around tens of micrometers, which is expensive to measure. We notice that there are several manufacturing factors that are related to the thickness variations of our sensors. Since our dataset is constructed by the sensors with different manufacturing settings, we improve our prediction systems by fusing the varying manufacturing factors to the inputs of prediction system. In our case, two essential manufacturing factors described below will be used.

- Solid content: One property in the solution recipe of making the ISM. It represents the percentage by weight of the

coating solution that is non-solvent. The range of the solid contents in our dataset is $[22.08, 31.51]$ %.

- Flow rate: It records the speed of coating in the fabrication process. The range of the flow rate in our dataset is $[0.4, 1.4]$ mL/min.

To efficiently fuse the above manufacturing factors with the image data, we concatenate the array of 2-element manufacturing factors and the extracted 9-element LBP array. In addition, we normalize both features to balance the weights of these two inputs. In particular, the sum of elements in each LBP array is equal to 1. Also, we normalize the manufacturing factors to the range 0 to 1. The normalized features will be the new inputs fed to two independent SVRs for predicting a and b.

We also propose a method to fuse the manufacturing features and our CNN's visual features to leverage the CNN's ability for feature extraction. Since the previous prediction method of tuning the CNN uses end-to-end training, that method is limited to directly fusing the 2D image and the 1D manufacturing features. As a alternative approach, we apply the architecture of ResNet-34 with weights pretrained on ImageNet to extract the visual features. There is only one FC layer in ResNet-34. In our implementation, all layers before the last FC layer are used for feature extraction. The output visual features comprise a 512-element array. Normalization is applied to the visual features and the manufacturing factors to balance the inputs. We concatenate them together and implement the same non-linear SVR system to realize the regression. Our experiments will quantify and compare the prediction system before and after fusing the manufacturing factors.

Experiments and Results

Following the methods for dataset generation discussed previously, we construct a dataset, including 123 sensors with the extracted active-region images and their sensor performance metrics. Then, the curve fitting method is applied to generate ground truth V_{fit} that can be described by parameters a and b in Eq. 2. We use root mean square error (RMSE) based on the difference between the fitted curve V_{fit} and the down-sampled measurement V_d to evaluate the performance of the curve fitting for each sensor, as shown in Eq. 4. Here, $N = 80$, which is the number of time points. The range of time points corresponds to the saturated phase of the raw data V_m. As a result, the average value of the RMSE is 2.72 mV or 2.83% for the whole dataset. In conclusion, the fitted logarithm curve V_{fit} can accurately depict the original measured potentiometric response in the saturated phase.

$$RMSE_{fit} = \sqrt{\frac{1}{N}\sum_{x_t=20}^{99}\left(V_d(x_t) - V_{fit}(x_t)\right)^2} \tag{4}$$

$$RMSE_{fit}(\%) = \sqrt{\frac{1}{N}\sum_{x_t=20}^{99}\left(\frac{V_d(x_t) - V_{fit}(x_t)}{V_d(x_t)}\right)^2} \times 100\% \tag{5}$$

We use 6-fold cross validation, one of techniques in machine learning evaluation, to prevent over-fitting and to provide a fair comparison of each method. To perform this technique, we randomly separate our dataset into 6 folds with 20, 20, 20, 20, 20, and 23 sensors in each fold. In each experiment, we pick 5 folds for training a prediction model. Then, the remaining 1 fold, which was not used in training, is used to inference the trained model. From the 6 experiments with different inference datasets, the average and variance of the results will be calculated to evaluate the prediction methods. We apply cross validation for each method to quantify the prediction accuracy and variance in a production environment.

Implementation Details

We follow the above experimental procedure for both our traditional machine learning and CNN based methods to predict the fitted logarithmic curve V_{fit} with the predicted parameters $\tilde{a}$ and $\tilde{b}$. We also fuse the thickness related manufacturing factors (MF) to the inputs of these two methods to compare with the prediction performance solely based on the sensor active-region image. In summary, we realize the prediction of sensor performance with the following four methods.

- **LBP + SVR** A 9-element 1D LBP texture representation is extracted from the active-region image and fed to the SVR. Since SVR assumes that the input features are in the standard range 0 to 1, a normalization process for the 1D LBP feature vector mapping the minimum and maximum to 0 and 1, respectively, is performed before feeding the images to the training process. In addition, as we mentioned earlier, there are two flexible hyper-parameters in the training process, the margin ε and the weight of the penalty C. A larger weight of penalty and a smaller margin makes the model less tolerant of deviations, and vice versa. Here, we select $C = 2 \cdot 10^3$, and $\varepsilon = 10^{-2}$ from trials for both SVR systems of predicting a and b. In addition, for a fair comparison these hyper-parameters are fixed in our 6-fold cross-validation experiments.
- **Fine-tuned CNN** To implement this end-to-end deep learning approach, the active-region image is directly fed to ResNet-34. In this implementation, the ImageNet pretrained weights are the initial weights of our model. As our dataset is small, a small learning rate 10^{-5} is used in training. In addition, the batch size is 4, which means that we select 4 training examples for each forward/backward pass. The model is trained for 5K epochs for stable performance. The Fine-tuned CNN method requires a GPU for efficient computation. We implement this method with Pytorch, which is an open source machine learning library.
- **LBP + MF + SVR** The 2-element manufacturing factor vector is concatenated with the 9-element LBP array. Then, we perform the training and inference in the same manner as we did for LBP + SVR, but with the different inputs. In this method, we optimize C to be $2 \cdot 10^4$, and ε to be 10^{-2}.
- **Pre-trained CNN + MF + SVR** This method also leverages the architecture of ResNet-34. In contrast to Fine-tuned CNN, there are no hyper-parameters to set for training. All the layers' parameters are pretrained on ImageNet and frozen during the CNN feature extraction. The normalized 512-element output from the last average pooling layer is concatenated with the normalized 2-element manufacturing factor vector as the overall feature vector. The subsequent SVR systems predict the parameters a and b based on the new features. Since the SVR is sensitive to its hyper-parameters, we adjust C and ε to be $2 \cdot 10^4$ and 10^{-3}, respectively, to implement this method.

Evaluation and Results

The inference phase computes the predicted curve $\tilde{V}_{fit}$ and compares it with the ground truth, which is the fitted logarithm curve V_{fit}. We use RMSE and its percentage to quantify the prediction error between these two curves that are a function of time.

Eq. 6 and Eq. 7 show the computation formulas. For each of the above four methods, we apply the experiments of 6-fold cross validation with the same data sets in each fold for fair comparison. The average RMSE, the average RMSE in percentage, and the standard deviation of RMSE for the 6 experiments conducted with each of the 4 methods are shown in Table 1.

$$RMSE_{predict} = \sqrt{\frac{1}{N}\sum_{x_t=20}^{99}\left(V_{fit}(x_t) - \tilde{V}_{fit}(x_t)\right)^2} \tag{6}$$

$$RMSE_{predict}(\%) = \sqrt{\frac{1}{N}\sum_{x_t=20}^{99}\left(\frac{V_{fit}(x_t) - \tilde{V}_{fit}(x_t)}{V_{fit}(x_t)}\right)^2} \times 100\% \tag{7}$$

Table 1: Results of RMSE in four prediction methods with 6-fold cross-validation experiments.

Method	AVG [mV]	AVG [%]	STDEV [mV]
LBP+SVR	19.91	19.92	3.73
Fine-tuned CNN	14.66	14.71	2.79
LBP+MF+SVR	11.56	12.35	2.53
Pre-trained CNN+MF+SVR	11.27	11.04	1.98

In our results, the average RMSE represents the prediction accuracy. The standard deviation shows the robustness of the prediction method. From the comparison of the first row and the second row in Table 1, Fine-tuned CNN achieves better performance than LBP + SVR. This shows that the CNN can extract more reliable visual features and construct a more accurate regression model to predict the desired outputs. On the other hand, the implementation of our Fine-tuned CNN method is more expensive. It requires a GPU and takes around 2 hours to generate a single prediction model in the training phase. The SVR learning model takes less than 0.01 seconds to generate the prediction model, which is much faster in the training phase. Also, tuning the CNN is designed to handle the image data solely; and it is limited to boosting accuracy by fusing additional data to the input images.

Since the SVR learning model is flexible with the input features, we analyze the effects of the different inputs by applying the SVR prediction systems. From the comparison between the prediction results of LBP + SVR and LBP + MF + SVR in Table 1, the traditional machine learning method achieves significantly higher accuracy and more robustness after fusing the manufacturing factors, which affect the thickness of the membrane. This comparison also verifies the physics-based assumption that thickness variations of the membranes strongly affect the sensor performance. In addition, the method of Pre-trained CNN + MF + SVR combines the CNN-based image features and the thickness-related data to the inputs and realizes the prediction by SVR model. This method reduces the RMSE of prediction error to 11.04% and achieves the most accurate and robust performance among the proposed prediction systems.

Conclusion

We exploit several different machine learning approaches to realize the prediction of the performance of thin-film soil nitrate sensors based on pre-processed sensor images and manufacturing factors. The physics-based model that the sensor response obeys a logarithmic curve as a function of time paves the way for our curve prediction. In this work, CNN shows a more powerful ability to extract accurate features from images that are related to sensor performance. The comparison among the different input features with the SVR system verifies that the thickness of the membrane strongly affects the sensor performance. In addition, fusing thickness-related manufacturing factors with the image-based features significantly improves the prediction performance and reduces the error to 11.04%. We also note from the third row versus the fourth row in Table 1 that feature fusion of manufacturing factors with a Pre-trained CNN achieves slightly better results than LBP + MF + SVR. In the future, we will focus on an efficient way to fuse manufacturing factors with the more reliable visual features provided by the Fine-tuned CNN. In addition, more manufacturing factors will be tailored and fed to the regression to improve prediction performance and monitor the manufacturing process.

References

[1] "SMART Films Consortium," Brick Nanotechnology Center, Purdue University, West Lafayette, IN. [Online]. Available: https://engineering.purdue.edu/SMART-consortium

[2] J. Hu, A. Stein, and P. Bühlmann, "Rational design of all-solid-state ion-selective electrodes and reference electrodes," *TrAC Trends in Analytical Chemistry*, vol. 76, pp. 102–114, 2016.

[3] Q. Yang, Y. Yan, K. Maize, X. Jin, H. Jiang, M. A. Alam, B. Ziaie, G. Chiu, A. Shakouri, and J. P. Allebach, "Image based quality assurance of fabricated nitrate sensor," *NIP & Digital Fabrication Conference*, 2019.

[4] T. Ojala, M. Pietikäinen, and T. Mäenpää, "Multiresolution gray-scale and rotation invariant texture classification with local binary patterns," *IEEE Transactions on Pattern Analysis & Machine Intelligence*, vol. 24, no. 7, pp. 971–987, 2002.

[5] H. Drucker, C. J. Burges, L. Kaufman, A. J. Smola, and V. Vapnik, "Support vector regression machines," *Advances in Neural Information Processing Systems*, pp. 155–161, 1997.

[6] L. Kang, P. Ye, Y. Li, and D. Doermann, "Convolutional neural networks for no-reference image quality assessment," *Proceedings of the IEEE Conference on Computer Vision and Pattern Recognition*, pp. 1733–1740, 2014.

[7] J. T. Stock and M. V. Orna, *Electrochemistry, past and present*. Washington, DC: American Chemical Society, 1989, vol. 390.

[8] N. Kanopoulos, N. Vasanthavada, and R. L. Baker, "Design of an image edge detection filter using the Sobel operator," *IEEE Journal of Solid-State Circuits*, vol. 23, no. 2, pp. 358–367, 1988.

[9] N. Otsu, "A threshold selection method from gray-level histograms," *IEEE Transactions on Systems, Man, and Cybernetics*, vol. 9, no. 1, pp. 62–66, 1979.

[10] S. Sedaghat, S. Jeong, A. Zareei, S. Peana, N. Glassmaker, and R. Rahimi, "Development of a nickel oxide/oxyhydroxide-modified printed carbon electrode as an all solid-state sensor for potentiometric phosphate detection," *New Journal of Chemistry*, vol. 43, no. 47, pp. 18 619–18 628, 2019.

[11] J. J. Moré, "The Levenberg-Marquardt algorithm: implementation and theory," in *Numerical analysis*. Berlin, Heidelberg: Springer, 1978, pp. 105–116.

[12] T. Ojala, M. Pietikäinen, and T. Mäenpää, "A generalized local binary pattern operator for multiresolution gray scale and rotation invariant texture classification," *International Conference on Advances in Pattern Recognition*, pp. 399–408, 2001.

[13] B. Scholkopf, K.-K. Sung, C. J. Burges, F. Girosi, P. Niyogi, T. Pog-

gio, and V. Vapnik, "Comparing support vector machines with Gaussian kernels to radial basis function classifiers," *IEEE Transactions on Signal Processing*, vol. 45, no. 11, pp. 2758–2765, 1997.

[14] K. He, X. Zhang, S. Ren, and J. Sun, "Deep residual learning for image recognition," *Proceedings of the IEEE Conference on Computer Vision and Pattern Recognition*, pp. 770–778, 2016.

[15] K. Simonyan and A. Zisserman, "Very deep convolutional networks for large-scale image recognition," *arXiv preprint arXiv:1409.1556*, 2014.

[16] A. Krizhevsky, I. Sutskever, and G. E. Hinton, "ImageNet classification with deep convolutional neural networks," *Advances in Neural Information Processing Systems*, pp. 1097–1105, 2012.

[17] J. Deng, W. Dong, R. Socher, L.-J. Li, K. Li, and L. Fei-Fei, "ImageNet: A large-scale hierarchical image database," *Proceedings of the IEEE Conference on Computer Vision and Pattern Recognition*, pp. 248–255, 2009.

Author Biography

Qingyu Yang *received her B.S.(2017) and M.S. (2019) in Electrical Engineering from Purdue University and currently is Ph.D. candidate in Purdue ECE. Her research focuses on image quality analysis, computer vision, object detection, and deep learning applications.*

Kerry Maize *received his B.S. in Electrical Engineering and Computer Science from UC Berkeley in 2002. He came to UCSC in 2005 to pursue graduate study in the areas of quantum electronics and nanoscience. His current work is focused on optical coherence tomograohy, and thermal device characterization. Prior to engineering Kerry worked in journalism.*

Xin Jin *received his Ph.D. degree from Purdue ECE in Feb. 2020. His research interests include design and analysis of next generation electrochemical bio-sensors for IoT applications.*

Hongjie Jiang *joined Professor Babak Ziaie group at August 2013 and received his Doctoral degree at October 2018 from ECE Purdue. Currently he works in ShenZhen msu-bit university. His research interests include sensor and actuator, microfluidics, printed electronics, bioMEMS, etc.*

Muhammad Ashraful Alam *holds the Jai N. Gupta Endowed Chair professorship at Purdue University, where his research focuses on the physics and technology of semiconductor devices. From 1995 to 2003, he was with Bell Laboratories, Murray Hill, NJ working on optoelectronic integrated circuits. Since joining Purdue in 2004, Dr. Alam has published over 300 papers on biosensors, transistors, solar cells, and flexible electronics. He is a fellow of IEEE, APS, and AAAS.*

Rahim Rahimi *received his PhD in electrical engineering from Purdue University, West Lafayette, IN, USA, in 2017. From 2018 to 2019, he was a Postdoctoral Researcher with the Biomedical Engineering Department at Purdue University. Since 2019, he has been an Assistant Professor in the materials science engineering at Purdue University. His current research focus is on developing innovative tools and technologies that can be utilized in solving various obstacles in healthcare, agriculture, and the environment.*

George T.C. Chiu *is a Professor of Mechanical Engineering with courtesy appointments in Electrical and Computer Engineering and Psychological Sciences at Purdue University. He received the B.S. degree from National Taiwan University and the M.S. and Ph.D. degrees from University of California at Berkeley. His research interests are mechatronics and control with applications to digital printing and imaging systems, digital fabrications and functional printing. He is a Fellow of ASME and IS&T.*

Ali Shakouri *is a professor of electrical and computer engineering and director of Birck Nanotechnology Center at Purdue University. He received his PhD from Caltech. His current research is on nanoscale heat transport and electrothermal energy conversion. He has developed lock-in imaging for temperature measurement and for real-time monitoring of functional film manufacturing. He is also leading a team to manufacture low-cost smart internet of thing (IoT) devices and sensor network for applications in advanced manufacturing and agriculture.*

Jan P. Allebach *is Hewlett-Packard Distinguished Professor of Electrical and Computer Engineering at Purdue University. Allebach was named Electronic Imaging Scientist of the Year by IS&T and SPIE, and was named Honorary Member of IS&T, the highest award that IST bestows. He has received the IEEE Daniel E. Noble Award, the IS&T/OSA Edwin Land Medal, is a Fellow of the National Academy of Inventors, and is a member of the National Academy of Engineering.*